Protein Science (2000), *9*:37–48. Cambridge University Press. Printed in the USA.
Copyright © 2000 The Protein Society

Expression, purification, and structural analysis of the trimeric form of the catalytic domain of the *Escherichia coli* dihydrolipoamide succinyltransferase

JAMES E. KNAPP,[1] DONALD CARROLL, JANET E. LAWSON, STEPHEN R. ERNST, LESTER J. REED, AND MARVIN L. HACKERT

Department of Chemistry and Biochemistry, The University of Texas at Austin, Austin, Texas 78712

(RECEIVED July 13, 1999; FINAL REVISION October 13, 1999; ACCEPTED October 14, 1999)

Abstract

The dihydrolipoamide succinyltransferase (E2o) component of the α-ketoglutarate dehydrogenase complex catalyzes the transfer of a succinyl group from the *S*-succinyldihydrolipoyl moiety to coenzyme A. E2o is normally a 24-mer, but is found as a trimer when E2o is expressed with a C-terminal $[His]_6$ tag. The crystal structure of the trimeric form of the catalytic domain (CD) of the *Escherichia coli* E2o has been solved to 3.0 Å resolution using the Molecular Replacement method. The refined model contains an intact trimer in the asymmetric unit and has an *R*-factor of 0.257 (R_{free} = 0.286) for 18,699 reflections between 10.0 and 3.0 Å resolution. The core of tE2oCD (residues 187–396) superimposes onto that of the cubic E2oCD with an RMS difference of 0.4 Å for all main-chain atoms. The C-terminal end of tE2oCD (residues 397–404) rotates by an average of 37° compared to cubic E2oCD, disrupting the normal twofold interface. Despite the alteration of quaternary structure, the active site of tE2oCD shows no significant differences from that of the cubic E2oCD, although several side chains in the active site are more ordered in the trimeric form of E2oCD. Analysis of the available sequence data suggests that the majority of E2 components have active sites that resemble that of *E. coli* E2oCD. The remaining E2 components can be divided into three groups based on active-site sequence similarity. Analysis of the surface properties of both crystal forms of *E. coli* E2oCD suggests key residues that may be involved in the protein–protein contacts that occur between the catalytic and lipoyl domains of E2o.

Keywords: crystal structure; dihydrolipoamide succinyltransferase; multienzyme complexes; X-ray crystallography

The family of α-keto acid dehydrogenase multienzyme complexes includes the α-ketoglutarate dehydrogenase complexes (KGDC), the pyruvate dehydrogenase complexes (PDC), and the branched-chain α-keto acid dehydrogenase complexes (BCKDC). Each complex is composed of multiple copies of three enzymes: a substrate-specific decarboxylase-dehydrogenase (E1), a distinct dihydrolipoamide acyltransferase (E2), and a common dihydrolipoamide dehydrogenase (E3) (Patel & Roche, 1990; Reed & Hackert, 1990; Perham, 1991).

Each complex is assembled around a core composed of either 24 E2 subunits arranged with octahedral symmetry (point group 432) or 60 E2 subunits arranged with icosahedral symmetry (point group 532). Multiple copies of E1 and E3 bind to this core to form the active complex.

The E2 component is a modular protein that is composed of one, two, or three amino-terminal lipoyl domains, followed by an E1- and/or E3-binding domain, and then by a carboxyl-terminal catalytic domain. The domains are connected by linker segments (Reed & Hackert, 1990; Perham, 1991). The flexibility of the linker segments is thought to inhibit crystallization of the native E2. Despite this setback, a significant amount of structural information has been obtained from analysis of the individual domains. The NMR structures of several lipoyl and E3-binding domains have been reported (Robien et al., 1992; Dardel et al., 1993; Kalia et al., 1993; Green et al., 1995; Berg et al., 1996, Ricaud et al., 1996). The crystal structure of the 24-mer inner core of the *Azotobacter vinelandii* dihydrolipoamide acetyltransferase (E2pCD) has been solved in the presence (Mattevi et al., 1993a) and absence (Mattevi et al., 1992, 1993b) of substrate. In addition, the crystal structures of the 24-mer inner core of the *Escherichia coli* dihydrolipoamide succinyltransferase (E2oCD) (Knapp et al., 1998) and the 60-mer inner cores of the *Bacillus stearothermophilus* and *Enterococcus faecalis* dihydrolipoamide acetyltransferases have been reported (Izard et al., 1999).

Reprint requests to: Marvin L. Hackert, Department of Chemistry and Biochemistry, The University of Texas at Austin, Austin, Texas 78712; e-mail: m.hackert@mail.utexas.edu.

[1] Present address: University of Massachusetts Medical Center, 373 Plantation St., Biotech II, Worcester, Massachusetts 01605.

Abbreviations: CAT, chloramphenicol acetyltransferase; CD, catalytic domain; cE2oCD, cubic E2oCD; tE2oCD, trimeric E2oCD; RMSD, root-mean-square deviation.

The catalytic domain of the E2o (E2oCD), like that of the *A. vinelandii* E2pCD, forms tightly associated trimers arranged at the corners of a cube to form a 24-mer with 432 symmetry. The last seven residues from one subunit interact with helices H2, H3, and H4 from a twofold symmetry-related subunit (Knapp et al., 1998). The addition of a $[His]_6$ tag to the C-terminus disrupts the twofold interactions so that E2oCD now exists as a trimer (tE2oCD) in solution. In this paper, we report the crystal structure of the *E. coli* tE2oCD expressed with a C-terminal His tag. Several side chains are visible in the electron density of this trimeric form of E2oCD that were disordered in the cubic crystal form of E2o. Furthermore, an examination of the electrostatic surfaces of this model led to the identification of a set of interactions that are likely to occur between E2oCD and its lipoyl domain.

Results

The refined model

The trimeric form of the catalytic domain of the *E. coli* E2o (tE2oCD) crystallized in space group $P3_121$ with a trimer of 759 residues, six sulfate ions, and 28 water molecules in the asymmetric unit. Each subunit of the trimer includes residues 165–404 plus an additional 13 residues $[Q(A)_4\ LE(H)_6]$ harboring the 6 × His tag. The first and last residues visible in the electron density maps vary from subunit to subunit, presumably due to crystal contacts. The residues associated with the His tag are not seen in the electron density. The occupancies of 22 residues have been set to zero due to a total absence of electron density in a σ_A weighted $2F_o - F_c$ map contoured at 0.5σ. In addition, seven residues have been truncated to glycines, 45 residues have been truncated to alanines, and eight residues have been truncated by one or more atoms due to the lack of side-chain electron density. In the final model, subunit A consists of residues 173–401, subunit B of residues 175–402, and subunit C of residues 172–403. This model has an R_{factor} of 0.257 and a R_{free} of 0.286 for all the measured reflections between 10.0 and 3.0 Å resolution (Tables 1 and 2). The Ramachandran plot shows that 90.3% of the nonglycine/nonproline residues in tE2oCD have dihedral angles in the most favored regions of the plot. No residue has a dihedral angle that lies in the disallowed regions of the Ramachandran plot.

Quaternary structure

In both the cubic form of E2oCD (cE2oCD) and the trimeric form (tE2oCD), the trimer appears as a thick disk with a diameter of 70 Å and a height of 50 Å. Unexpectedly, the trimer in this crystal form does not have ideal threefold symmetry. The refinement of tE2oCD with NCS restraints, but not threefold restraints, using the conjugate-gradient energy-minimization routines of X-PLOR caused subunit A to reorient by 1.7° from ideal threefold symmetry, thereby removing unfavorable contacts between crystallographically related trimers. The omission of the residues that participate in the unfavorable crystal contacts did not prevent the deviation of tE2oCD from ideal threefold symmetry during the energy minimization protocol. Analysis of the refinement protocols clearly indicate that the deviation of subunit A from ideal symmetry is due to the minimization of the X-ray energy terms and not to the minimization of the geometric or NCS energy term. Looking down the molecular threefold axis of the trimer as viewed in Figure 1, subunit B (blue) is related to subunit A (purple) by a 121.7° clockwise rotation, whereas subunit C (red) is related to A by a 118.3° counterclockwise rotation. Subunit B is related to C by a 120.0° clockwise rotation. The 1.7° deviation of subunit A from ideal threefold symmetry shifts its backbone by an average of 0.27 Å per Cα atom with a maximum shift of 0.81 Å. It should be emphasized that the residues in the crystal contact region of the refined model adequately fit the electron density from a simulated annealing $2F_o - F_c$ σ_A-weighted omit map.

Table 1. *Refinement statistics for the model of trimeric E2oCD*

Resolution range (Å)	10.0–3.0
Number of reflections ($F > 0.0$)	18,669
Number of nonhydrogen protein atoms	4,989
Number of nonhydrogen water atoms	28
Number of nonhydrogen sulfate atoms	30
R_{factor}	0.257 (0.339)[a]
R_{free}	0.286 (0.399)[a]
RMSD from ideal values	
Bond lengths (Å)	0.007
Bond angles (deg)	1.42
Dihedral angles (deg)	25.2
Improper angles (deg)	1.23
Mean *B*-factors (Å^2)	
Main-chain atoms	40.6
Side-chain atoms	53.3
Water atoms	35.6
Sulfate atoms	68.8

[a] Values for the highest resolution shell for data from 3.18–3.0 Å.

Noncrystallographic symmetry

Imposing strict noncrystallographic symmetry (NCS) on the model did not adequately describe the electron density surrounding the N-terminal segment (residues 172–187), a middle segment (residues 215–219), and the last few residues (396–403) of each subunit. Unfortunately, the modest resolution of the data suggested that it would not be justified to remove the NCS constraints for the

Table 2. *Statistics for the tE2oCD X-ray data set*

Resolution	Reflections	Completeness	R_{sym}
10.0–6.01	1,929	94.9	0.058
6.01–4.96	1,910	96.9	0.084
4.96–4.39	1,918	97.3	0.084
4.39–4.02	1,903	98.1	0.110
4.02–3.75	1,900	98.7	0.147
3.75–3.54	1,927	98.6	0.198
3.54–3.37	1,807	94.2	0.172
3.37–3.22	1,804	93.2	0.180
3.22–3.10	1,781	93.0	0.226
3.10–3.00	1,798	93.5	0.309
10.0–3.00	18,677	95.8	0.103

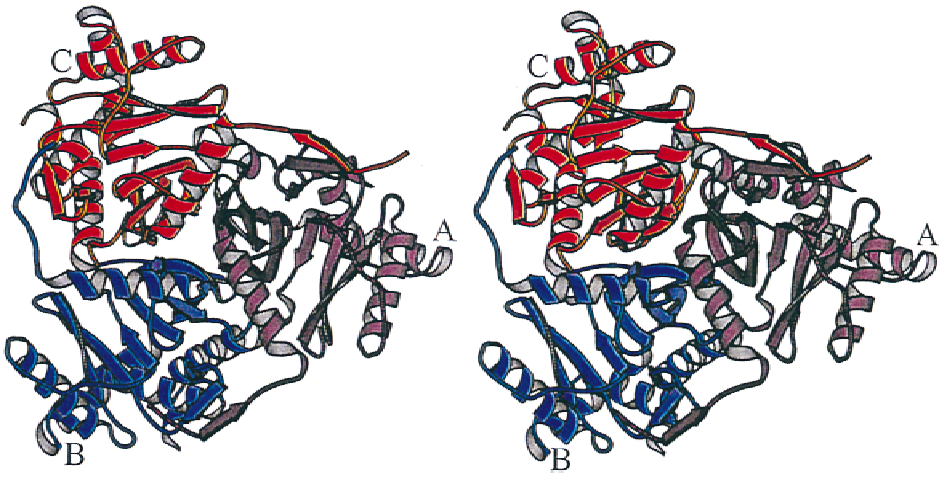

Fig. 1. The E2oCD trimer. The asymmetric unit of tE2oCD comprises three identical subunits that are labeled A (purple), B (blue), and C (red). The disk-shaped trimer is viewed down the molecular threefold axis from the side of the trimer that corresponds to the outside surface of the cubic E2oCD (Knapp et al., 1998). For consistency, all residues, including those that are disordered, were used to create this diagram.

entire trimer. As a compromise, tight NCS restraints (but not threefold symmetry) were applied to the model excluding those three segments. A total of 1,560 nonhydrogen atoms were tightly restrained during the last two rounds of refinement. Due to the tight restraints, the superposition of the NCS-restrained atoms of either subunits B or C onto those of subunit A resulted in an RMS difference of 0.009 Å. The nonrestrained atoms located in two of the segments (residues 215–219 and residues 396–403) showed only small differences between NCS related subunits, whereas the N-terminal segments showed much larger differences, probably caused by the asymmetry of crystal packing. Many of the residues in these regions interact with symmetry-related atoms only in one of the three subunits. However, the differences involving the residues in these segments suggest that the unrestrained parts of tE2oCD are free to assume a number of conformations (Fig. 2).

Subunit fold

Each tE2oCD subunit is composed of five α-helices (labeled H1, H2, H3, H4, and H6), one 3_{10} helix (labeled H5), and 10 β-strands (labeled A though J). Only subunit C retains the C-terminal 3_{10} helix (labeled H7), which was previously observed in the crystal structures of the cubic E2oCD (Knapp et al., 1998), and *A. vinelandii* E2pCD (Mattevi et al., 1992, 1993b). The secondary structural elements are arranged in two layers to form an open-faced sandwich motif (Richardson, 1981). One layer consists of a seven-stranded, central β-sheet (F$\downarrow$E$\uparrow$G$\uparrow$I$\uparrow$J$\downarrow$B$\uparrow$H′$\downarrow$), whereas the second layer consists of the five helical segments combined with a three-stranded, antiparallel β-sheet (A′$\downarrow$D$\uparrow$C$\downarrow$). Excluding the residues that are not defined, 1,096 main-chain atoms from subunit A, 1,054 atoms from subunit B, and 1,087 atoms from subunit C superimpose upon their counterparts in cE2oCD with RMS differences of 1.2, 0.8, and 1.2 Å, respectively (Fig. 2). If the superposition calculation is repeated using only the residues between Val187 and Asp396 while excluding all residues with a zero occupancy, 1,016, 994, and 997 main-chain atoms from subunits A, B, and C of tE2oCD superimpose upon the corresponding atoms in cE2oCD with RMS differences of 0.41, 0.39, and 0.41 Å, respectively. Thus, the largest differences between the two E2oCD structures are localized at the N- and C-terminal segments.

C-terminal residues and twofold contacts

Small changes in the position of the last seven residues of the tE20CD subunit prevent the trimers from assembling into the 24-mers observed previously (Knapp et al., 1998). The twofold interface is formed by insertion of the C-terminal tail from one subunit into a hydrophobic pocket formed by helices H2, H3, and H4 of the twofold-related subunit. The C-terminal ends of each subunit in tE2oCD are rotated by an angle between 29° and 45° relative to the corresponding residues in cE2oCD (Fig. 2B). It appears likely that the C-terminal His tag increases the flexibility of the C-terminal tail of tE2oCD, allowing these residues to assume a number of conformations. In support of this view, part of the C-terminal tail and the entire His tag are completely absent from the electron density.

The last few residues of each subunit that have reasonable electron density are stabilized by crystal contacts with a symmetry related molecule. The C-terminal ends of subunits A and C form a few crystal packing contacts, whereas the C-terminal end of subunit B makes a number of interactions with another trimer related by a crystallographic twofold. The subunit B–subunit B′ interface results in 519 Å^2 of solvent-accessible surface area buried per monomer. The large number of twofold contacts would be consistent with trimer–trimer interactions occurring in solution. A tendency of the trimer to aggregate on standing has been noted. It is interesting to note that this crystallographic twofold interface is quite similar to the molecular twofold interface of cubic E2oCD in that both E2oCDs are stabilized by contacts between the C-terminal ends of two subunits. The differences between the twofold interfaces of tE2oCD and cE2oCD arise from the rotation of the C-terminal residues by 29°. This rotation results in a 25.4° change in the orientation of the crystallographic twofold axis when compared to that of the cubic E2oCD, thereby preventing the E2oCD with a C-terminal His tag from forming the octahedral cube.

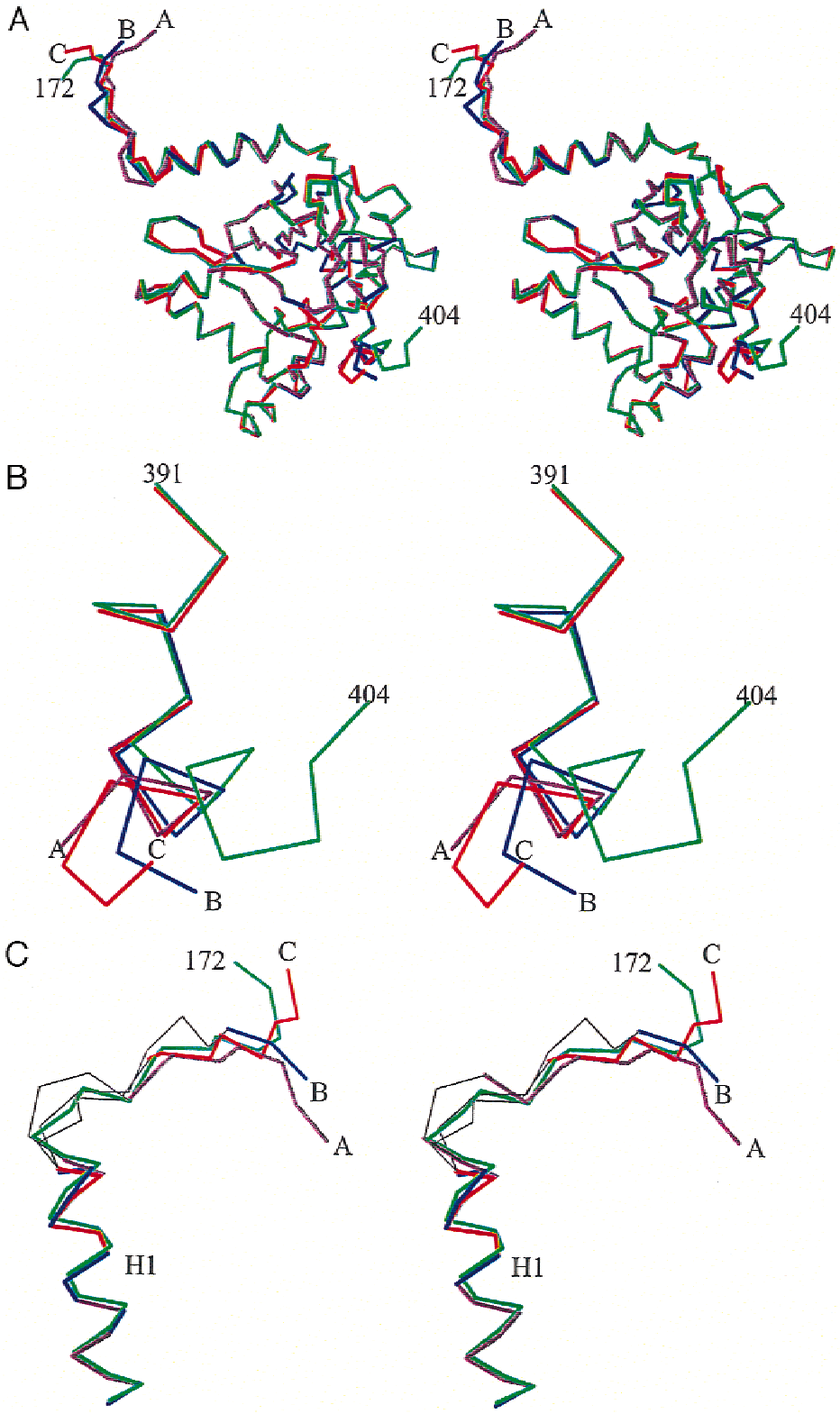

Fig. 2. The subunit fold of tE2oCD. **A:** The Cα traces of subunits A (purple), B (blue), and C (red) are superimposed on the Cα trace of cE2oCD (green). The largest differences between the four tE2oCD structures are localized at the N-terminal (residues 171–184) and C-terminal (residues 397–404) ends of E2oCD. **B:** A magnified view of the C-terminal ends of tE2oCD shows that the last visible residues of subunits A, B, and C are rotated by 37.9°, 29.0°, and 44.9°, respectively, when compared to the same residues of cE2oCD (green). In each case, the C-terminal segment is stabilized by contacts with a symmetry related trimer. **C:** A magnified view of the N-terminal ends of tE2oCD shows several other differences. Regions that include disordered residues are represented as thin black lines.

N-Terminal residues

A second region of tE2oCD that deviates from cE2oCD involves the first 12 residues visible in the electron density. This segment in cE2oCD includes β-strand A (residues 175–179) and the first turn of helix H1 (residues 182–184). β-Strand A of subunit C is similar to that of cE2oCD, whereas this strand of subunit A is truncated by one residue and is replaced by a random coil in subunit B. The first three residues visible in the electron density from C occupy similar positions as those of cE2oCD, whereas those from subunits A and B are both rotated by 141° with respect to the same residues of cE2oCD (Fig. 2C). The differences between the two crystal forms are likely due to differences in crystal packing contacts and not to a change in oligomeric state. In the cE2oCD structure, two of the first three residues (Arg173 and Ser174) participate in the packing of the E2oCD cubes within the crystal, whereas the residues of β-strand A form a number of contacts with the peripheral β-sheet from a threefold related subunit (Knapp et al., 1998). Only the N-terminal segment of subunit C of tE2oCD contacts a symmetry related trimer. The N-terminal segments of the other two subunits do not form crystal contacts, thus allowing the first three residues in the model to assume different conformations than those in the same region of subunit C.

Many of the residues in the second half of the N-terminal segment (residues 178–183) are disordered. The poor quality of electron density in this region of the three subunits resulted in the deletion of a total of 13 residues from the refined model. Part of the instability is probably due to the presence of several hydrophobic residues (Val178, Pro179, Met180, and Leu183), which are exposed to solvent. Poor quality of electron density was also observed in this region of the cubic E2oCD. Although Val178, Pro179, and Met180 of cE2oCD have well-defined electron density (due to contacts with a threefold-related subunit), several other residues in this region of the cE2oCD (Arg181, Arg182, Leu183, and Arg184) have side chains that are disordered.

Trimer contacts

tE2oCD is stabilized by a number of contacts involving 136 residues from the three subunits. The trimer interface buries 22.6% or 2,905 Å^2 of solvent accessible surface area per subunit. As in cE2oCD, the trimer interface of tE2oCD can be divided into four parts that are triplicated by the noncrystallographic symmetry. However, each of the threefold interfaces observed in tE2oCD differs from the others due to the flexibility of the N-terminal segment. The first part of the threefold interface in cE2oCD involves the interaction of β-strand A from one subunit with the peripheral β-sheet from the subunit related by a clockwise, threefold symmetry rotation. This β-strand A to β-strand D interaction is stabilized by nine hydrogen bonds, one of which is involved in a salt bridge between Arg177 and Asp256. Although β-strand A interacts with β-strand D in tE2oCD, the hydrogen bond pattern is somewhat different. β-strand A in subunit A of tE2oCD is oriented so that four hydrogen bonds are made with β-strand D of subunit B, whereas β-strand A of subunit B forms only two hydrogen bonds with subunit C. All but one of these hydrogen bonds are present in cE2oCD.

β-Strand A of subunit C forms nine hydrogen bonds with β-strand D of subunit B; however, only four of these hydrogen bonds are present in both E2oCD crystal structures. The salt bridge between Arg177–Asp256′ is also present at this interface. Two additional salt bridges, Arg172–Asp267′ and Lys184–Asp257′, not present in cE2oCD, stabilize this interface in tE2oCD. It is interesting to note that the Arg172–Asp267′ interaction is similar to the crystal contacts formed in the E2oCD crystals with F432 symmetry. In this case, Arg173 from one cube interacts with Asp267″ from a threefold related subunit on a different cube. A comparison of the three β-strand A–β-strand D interactions clearly shows that β-strand A can assume a number of conformations while still maintaining a number of contacts with its threefold related subunit. The requirement of the full-length E2o to assume a number of conformational states suggests that the flexibility of this region is functionally significant.

The remaining three sections of the threefold interface are quite similar to those observed in the cubic E2oCD. However, the side chain of Asn 196 from each subunit assumes a different position such that a hydrogen bond is formed between its Nδ1 atom and the Oδ2 atom of its counterpart from the counterclockwise, threefold-related subunit as defined in Figure 1. In addition, this interface is stabilized by a hydrogen bond between the Nδ2 atom of Asn195 from subunit A and the O atom from Asn195 from subunit C. The deviation of subunit A from threefold symmetry prevents the triplication of this hydrogen bond.

Active site

The active sites of both forms of E2oCD resemble those of chloramphenicol acetyltransferase (CAT) and *A. vinelandii* E2pCD. All three acyltransferases have active sites that are located by a substrate-binding channel formed between pairs of threefold related subunits, and thus are not adversely affected by the dissociation of the 24-mer into its trimeric components. The catalytic cycles of E2oCD and E2pCD are thought to proceed by a mechanism similar to that proposed for CAT (Guest, 1987; Shaw & Leslie, 1991). The first step of the E2oCD mechanism results in the deprotonation of the thiol group of coenzyme A by an active site histidine residue (His375 in E2oCD). The activated thiolate attacks the carbonyl carbon of the succinylated dihydrolipoyl moiety to form a tetrahedral intermediate. This intermediate is stabilized by the hydroxyl side chain of a threonine residue (Thr323′ in E2oCD), which is located on a threefold-related subunit. The breakdown of the tetrahedral intermediate results in the succinylation of coenzyme A and protonation of the dihydrolipoyl moiety. The active site histidine (His375) and threonine (Thr323′) residues differ from their counterparts in cE2pCD by less than 10° per torsion angle. However, one interesting difference is the presence of a large patch of electron density continuous with the end of the catalytic histidine from each subunit. A sulfate ion (one of the ions present in the crystallization solutions) was modeled into this density (Fig. 3).

The catalytic activity of E2oCD is thought to be dependent upon Asp379. The side chain of this residue is thought to interact with His375 and either Arg184 or Arg381 (Knapp et al., 1998). Asp379 is oriented with a χ1 angle of 64° in the trimeric structure, in good agreement with that observed in the cubic structure. This particular conformation positions the side chain of Asp379 away from the catalytic histidine. Although the χ2 angle of Asp379 in tE2oCD differs by 105° from its counterpart in the cubic E2oCD, this difference may be due to exposure of the side chain to solvent, which would increase the thermal motion of this residue. Both Arg184′ and Arg381 are disordered in cE2oCD, whereas both residues fit into adequate electron density in two out of the three tE2oCD subunits (Fig. 3). Arg381 and Arg184′ are both oriented

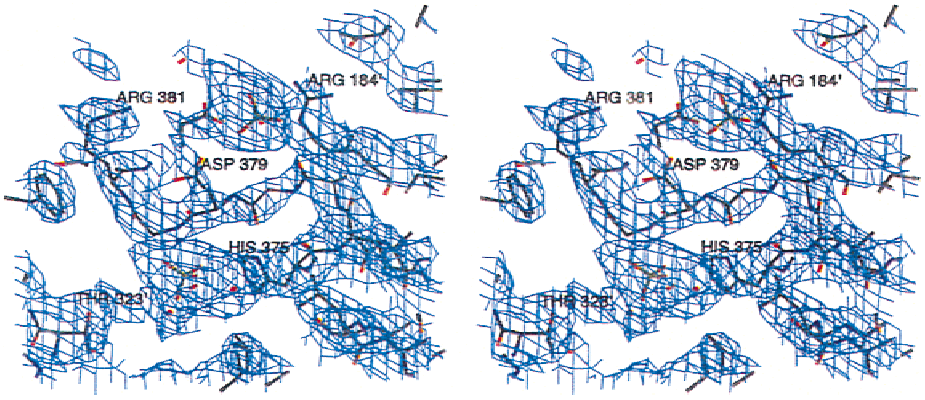

Fig. 3. The active site of tE2oCD. The tE2oCD model includes His375 from subunit A and Thr323′ from subunit C and is superimposed upon a $2F_o - F_c\ \sigma_A$ weighted map contoured at 1σ. Notice the continuous density connecting His375 with the sulfate ion. This ion is near the position that coenzyme A is expected to occupy when this substrate is being deprotonated by His375. Also notice that Asp379, Arg184′, and Arg381 are all pointing away from the active site histidine.

such that their side chains are pointing away from the catalytic histidine. In the case of Arg381, its guanidino group is positioned within 4.7 Å of the acidic side chains of Glu250 and Asp379.

By contrast, the equivalent aspartic acid residue in the liganded structures of CAT (Asp199) is oriented such that its Oδ1 atom is 3.4 Å away from the Nδ2 atom of its catalytic histidine (His196) (Leslie et al., 1988). In this particular conformation, Asp199 forms a salt bridge with Arg18. The Arg18–Asp199 salt bridge in CAT was originally thought to only maintain the structural integrity of the CAT active site (Gibbs et al., 1990). However, it has been suggested that this salt bridge exerts an electrostatic effect on the catalytic histidine (Hendle et al., 1995). The disruption of this salt bridge in CAT results in a decrease in k_{cat} (Lewendon et al., 1988), but causes only small changes in the CAT active site (Gibbs et al., 1990). Because of the orientations of Asp379, Arg184′, and Arg381 in tE2oCD, a similar salt bridge cannot be formed without a conformational change. It has been proposed that addition of substrate will cause Asp379 to alter its conformation, thus allowing an analogous salt bridge to form (Knapp et al., 1998). The tE2oCD structure confirms the previous observation that if a salt bridge is indeed required for catalytic activity, it must be formed upon substrate binding.

Discussion

Interactions involving the lipoyl domain

All E2 subunits contain a lipoyl moiety that is bound covalently in amide linkage to a specific lysyl residue in the lipoyl domain(s). Dihydrolipoamide can replace the covalently bound lipoyl moiety as substrate of E2 in vitro. The crystal structure of *A. vinelandii* E2pCD harboring dihydrolipoamide in the active site has been solved (Mattevi et al., 1993a). Based on this structure, dihydrolipoamide was modeled into the substrate-binding site of *E. coli* E2oCD (Knapp et al., 1998). We have used computer modeling to explore the binding of the lipoyllysyl moiety and adjacent amino acid residues to the active site of E2oCD.

Analysis of the electrostatic surface of E2oCD shows that a large electropositive patch surrounds the putative dihydrolipoamide-binding site. In contrast, the electrostatic surface of the lipoyl domain is mostly electronegative (Fig. 4A,B). These features should provide favorable protein–protein interactions. A model of this potential interaction is presented in Figure 5. The proposed lipoyl-catalytic domain interface could be stabilized by salt bridges formed between Arg177 and Glu47, Arg186 and Glu12, Arg190 and Asp42, and Arg284 and Glu40. Arg177 and Arg190 are present in all E2o sequences, whereas Arg186 and Arg284 are conserved in 10 and 9 of the 11 E2o sequences, respectively (Fig. 4D). All the E2o sequences surveyed have acidic side chains at positions 12, 40, and 42, whereas only 7 out of 11 sequences have an acidic side chain at position 47 (Fig. 4C).

The proposed interactions between catalytic and lipoyl domains do result in two sets of unfavorable interactions: one between Asp16 and Glu313, and the other between Glu38 and Glu175. Although the E2oCD–E2oLD model brings two pairs of acidic residues in close proximity to each other, the side chains of these acidic residues can move to positions that minimize electrostatic repulsion. It should be possible in future studies to evaluate the significance of these observations using site-directed mutagenesis.

Classification of E2 components

In addition to classifying the various E2 components into groups based on substrate specificity and oligomeric architecture, the E2 components can be categorized based on active site residues. Hendle et al. (1995) presented three models describing the active sites of different E2 components. However, the alignment of 51 presently known E2 sequences and two E2-like domains suggests that four active site groupings exist (Fig. 6). The first group includes the E2ps from the Gram-negative bacteria *A. vinelandii* (Hanemaaijer et al., 1988) and *Pseudomonas aeruginosa* (Rae et al., 1997). Each member of this group possesses Asn instead of Asp at residue 379 in E2oCD. The replacement of the active site asparagine (Asn614) with an aspartic acid in the *A. vinelandii* E2pCD results in a 8.5-fold decrease in k_{cat} accompanied by a 2.5-fold increase in the K_m for coenzyme A and a 1.7-fold decrease in the K_m for dihydrolipoamide (Hendle et al., 1995). The N-terminal domain of the α-ketoglutarate dehydrogenase (E1o) components from *Mycobacterium tuberculosis* (Philipp et al., 1996) and *Corynebacterium glutamicum* (Usuda et al., 1996) has significant homology to the

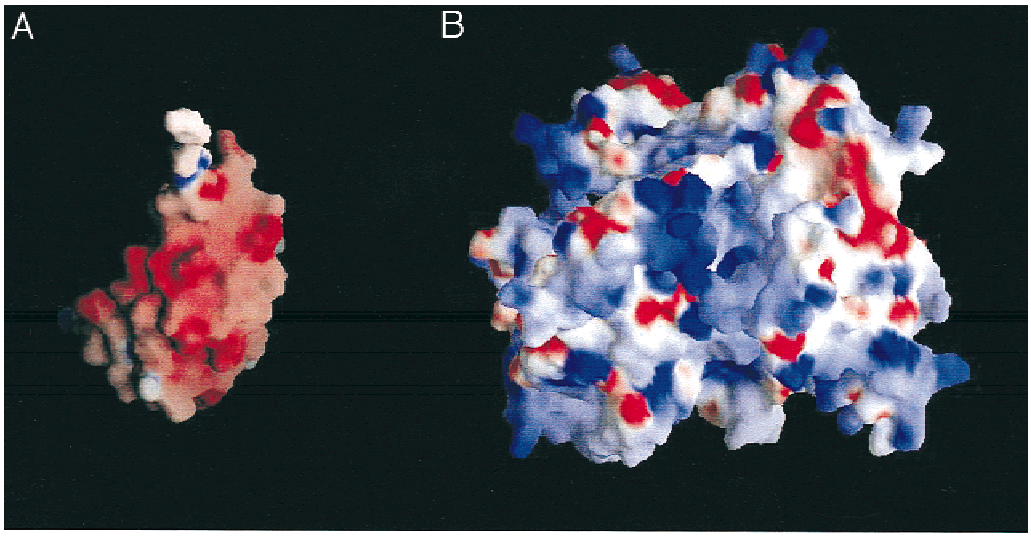

C E2o Lipoyl Domains

```
Eco    1-SSVDILVPDLPESVADATVATWHKKPGDAVVRDEVLVEIETDKVVLEVPASADGILDAVLED- 67
Avi    1-A-IDIKAPTFPESIADGTVATWHKKPGEPVKRDELIVDIETDKVVMEVLAEADGVIAEIVKN- 66
Bsu    1-KMAEIKVPELAESISEGTIAQWLKQPGDYVEQGEYLLELETDKVNVELTAEESGVLQEVLKD- 67
Sce   72-KSTSIEVPPMAESLTEGSLKEYTKQPGDFIKEDELLATIETDKIDIEVNSPVSGTVTKLNFK-134
Hum   68-DLVTVKTPAFAESVTEGD-VRWEKAVGDTVAEDEVVCEIETDKTSVQVPSPANGVIEALLVP-128
```

D E2o Catalytic Domains

```
Eco  180-MTRLRKRVAERLLEAKN-196    260-VVYHNYFDVSMAVSTPRGLVTPVLRDVDTLGM-291
Avi  173-MTRLRAKVAERLVEAQS-189    254-IVYHGYQDIGVAVSSDRGLVVPVLRNAEFMSL-285
Bsu  191-MSRRRQTIAKRLVEVQQ-207    272-LIVKKFYDIGIAVAAVEGLVTPVVRDADRLTF-303
Sce  240-MNRMRLRIAERLKESQN-256    320-IVYRDYTDISVAVATPKGLVTPVVRNAESLSV-351
Hum  226-MNRMRQRIAQRLKEAQN-242    309-VVYRDYIDISVAVATPRGLVVPVIRNVEAMNF-340
```

Fig. 4. The electrostatic potentials of the surface of the (**A**) *E. coli* E2o lipoyl domain (E2oLD) and that of the (**B**) E2oCD trimer. Negative, neutral, and positive potentials are shown in red, white, and blue, respectively. The surface surrounding the *S*-succinyldihydrolipoamide binding site of E2oCD (central cavity of the E2oCD trimer) includes a number of basic residues, whereas the surface of the lipoyl domain is negatively charged. The sequence alignment of the (**C**) lipoyl and (**D**) catalytic domains from selected E2o components shows the conserved acidic (red) and basic (blue) residues. As a reference, the lipoylated lysine is shown in bold black. This alignment included the sequences of E2os from *E. coli* (Eco) (Spencer et al., 1984), *A. vinelandii* (Avi) (Westphal & de Kok, 1990), *Bacillus subtilis* (Bsu) (Carlsson & Hederstedt, 1989), *Saccharomyces cerevisiae* (Sce) (Repetto & Tzagoloff, 1990), and human (Hum) (Ali et al., 1994).

catalytic domain of dihydrolipoamide acyltransferases. The active site residues of the E2o-like catalytic domains of both of these E1o complexes include a Gln at the position corresponding to Asp379 in E2oCD.

The E2ps from the Gram-negative bacteria *E. coli* (Stephens et al., 1983) and *Haemophilus influenzae* (Fleischmann et al., 1995) form the second group. These E2ps have an Asp at the position corresponding to Asp379 in E2oCD and contain Gln or Asn, respectively, at the position corresponding to Arg184 in E2oCD. A computer model of the *E. coli* E2p-active site suggests that Arg475 (position 250 in the E2oCD numbering scheme) can interact with the active site aspartic acid (Hendle et al., 1995). Therefore, this residue may function in the same way as Arg184 in E2oCD.

The third and largest of the four groups is represented by 42 sequences, and includes all known E2os, bacterial E2bs, and E2ps from Gram-positive bacteria and eukaryotic species. The E2s of this group are characterized by an active site that resembles that of the *E. coli* E2oCD. All E2s of this group have an aspartic acid at the position corresponding to Asp379 in E2oCD. All but two members of this group have Arg at the position corresponding to Arg184 in E2oCD. The two exceptions, the E2p from *Alcaligenes eutrophus* (Hein & Steinbüchel, 1994) and *Neisseria meningitidis* (Ala' Aldeen et al., 1996), have Lys in place of Arg. Lysine should be capable of interacting with the active site aspartic acid in a manner similar to arginine.

The last group of dihydrolipoamide acyltransferases is composed of the eukaryotic E2bs. The active sites of these E2s resemble the active sites of the E2s comprising Groups II and III in that they retain the active site Asp, but differ in that the active sites of the Group IV E2s do not harbor a basic residue near the active site Asp. Although human and mouse E2b components contain Gln at the position equivalent to Arg184, it is doubtful that this residue could interact with its active site Asp. All known eukaryotic E2bs encode either Lys or Arg adjacent to the Gln. If helix H1 is rotated about its long axis, the base at position 185 would be able to interact with the active site aspartic acid. It should be noted that

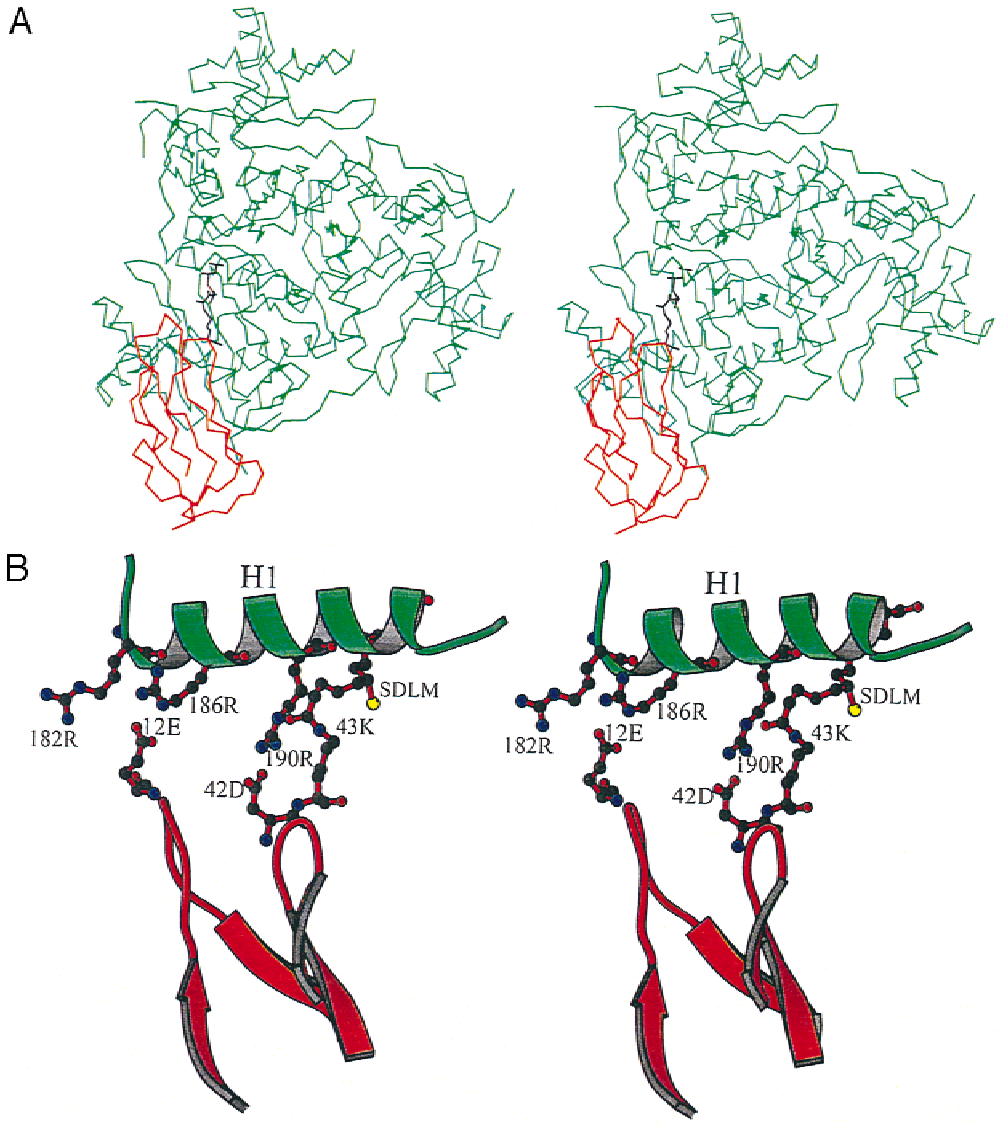

Fig. 5. A model for the E2oCD–E2oLD interface. **A:** This view shows the proposed interaction between the lipoyl domain of *A. vinelandii* E2p(red) (Berg et al., 1996) and the *E. coli* E2oCD trimer (green). The *S*-succinyldihydrolipoyl moiety (SDLM) is attached to Lys42. **B:** The lipoyl domain is recognized by Arg186, Arg190, Arg283 (not shown), and Arg176′ (not shown) of E2oCD. Arg186 interacts with Glu12, whereas Arg190 interacts with Asp42.

helix H1 from all eukaryotic E2b components is truncated by one residue compared to helix H1 from other E2 sequences. This deletion could rotate helix H1, allowing Arg/Lys185 to perform the analogous function as Arg184 in E2oCD.

Materials and methods

Materials

Plasmid pGS490, containing nucleotides 3392 to 4360 of the *E. coli sucB* gene (Spencer et al., 1984), was provided by Drs. John R. Guest and George C. Russell, succinyl-CoA synthetase was from Dr. Jonathan S. Nishimura, and plasmid pGroESL was from Dr. George Lorimer. Plasmids pET-21a(+) and pET-32a(+) were obtained from Novagen (Madison, Wisconsin).

Vector construction and expression

A DNA fragment encoding amino acid residues 93 to 404 of E2o, lacking the lipoyl domain, was amplified by the polymerase chain reaction from pGS490 using specific oligonucleotide primers. These primers introduced an *Eco*RI site at the 5′ end and a *Hin*dIII site at the 3′ end of the subgene. The DNA fragment was sequenced to confirm its identity. The restriction sites were used to subclone the DNA fragment into pET-21a(+) and into a modified pET-32a(+). The former vector carries a C-terminal 6 x His tag sequence, whereas the latter vector carries an N-terminal 6 x His tag sequence. *E. coli* strain BL21(DE3) was cotransformed with each plasmid separately plus pGroESL, which encodes the chaperonin proteins groEL and groES. Double transformants were selected on media containing 50 μg/mL ampicillin and 50 μg/mL chloramphenicol. Cultures of transformed cells were grown under condi-

Group	Source	Region 1	Region 2	Region 3	Region 4	Reference
		182 191	249 251	275 277	373 382	
I	Avi E2p	RLMQIGZTNL	PDF	PDG	YDHRVINGAA	Hanemaaijer et al., 1988
I	Pae E2p	RLIEVGAANL	PDF	PDG	YDHRVINGAA	Rae et al., 1997
II	Eco E2p	RIQKISGANL	PRF	PNG	FDHRVIDGAD	Stephens et al., 1983
II	Hin E2p	RINKISGANL	PRF	PNG	FDHRVIDGAD	Fleishmann et al., 1995
III	Aeu E2p	RIKKISGANL	PNF	PNG	WDHRVIDGAE	Hein & Steinbüchel, 1996
III	Bst E2p	GIRKAIAKAM	PVL	EKG	FDHRMIDGAT	Borges et al., 1990
III	Nme E2p	RIKKISGQNL	PEF	PNG	FDHRVIDGAA	Ala' Aldeen et al., 1996
III	Sce E2p	TMRSIIGERL	PDA	PTG	FDHRVVDGAV	Niu et al., 1988
III	Hum E2p	NIRRVIAQRL	PEA	PAG	CDHRVLDGLV	Thekkumkara et al., 1988
III	Eco E2o	RLRKRVAERL	PEV	PRG	YDHRILDGRE	Spencer et al., 1984
III	Hin E2o	RLRKRIAERL	PEV	PRG	YDHRLIDGRE	Fleishmann et al., 1995
III	Avi E2o	RLRAKVAERL	PGV	PRG	YDHRLIDGKE	Westphal & de Kok, 1990
III	Bsu E2o	RRRQTIAKRL	PLL	VEG	YDHRIVDGKE	Carlsson & Hederstedt, 1993
III	Sce E2o	RMRLRIAERL	PAV	PKG	YDHRLLDGEK	Repetto & Tzagoloff, 1990
III	Hum E2o	RMRQRIAQRL	PVV	PRG	YDHRLIDGRE	Nakano et al., 1993
III	Ppu E2b	GLRRKIAQRM	PQI	DNG	FDHRVVDGMD	Burns et al., 1988
III	Bst E2b	GVRKAIASNM	PQM	EDS	LDHRVLDGLV	Wang et al., 1993
IV	Bov E2b	GFQKAMVKTM	PIL	EQG	ADHRIIDGAT	Griffin et al., 1988
IV	Hum E2b	GFQKAMVKTM	PIL	EQG	ADHRVIDGAT	Lau et al., 1992

Fig. 6. The alignment of the active site regions from selected E2 catalytic domains. The E2 sequence alignment suggests that all known E2 catalytic domains can be assigned to one of four groups on the basis of active site residues. E2s of Group I encode an asparagine at position 379, whereas E2s of groups II, III, and IV encode an aspartic acid at this position. The active site aspartic acid is thought to interact with a basic residue at either position 250 (Group II), 184 (Group III), or 185 (Group IV). This alignment includes the sequences of the E2o, E2p, and E2b from *Homo sapian* (Hum); the E2o and E2p from *E. coli* (Eco), *H. influenzae* (Hin), *A. vinelandii* (Avi), and *S. cerevisiae* (Sce); the E2p and E2b from *B. stearothermophilus* (Bst); the E2p from *Pseudomonas aeruginosa* (Pae), *A. eutrophus* (Aeu), and *N. meningitidis* (Nme); the E2o from *B. subtilis* (Bsu); and the E2b from *Pseudomonas putida* (Ppu), and *Bos taurus* (Bov). The sequences were aligned using Macaw version 2.0.5 (Schuler et al., 1991). The numbering scheme refers to the amino acid sequence of the catalytic domain of *E. coli* E2o CD.

tions optimal for expression of soluble truncated E2o as determined by SDS-PAGE and by assay of E2 activity (Knight & Gunsalus, 1962).

Purification and characterization of truncated E2o

Transformed cells were grown on LB medium containing 50 μg/mL ampicillin and 50 μg/mL chloramphenicol at 37 °C to an A_{595} of 0.5. Expression was induced by addition of isopropyl β-thiogalactoside to a final concentration of 50 μM. Incubation was continued for 8 h at 20 °C before harvesting. The cells were disrupted in a French pressure cell. The two truncated E2os were purified to near homogeneity by affinity chromatography on Ni^{2+}-nitriloacetic-agarose beads by procedures described previously (Maeng et al., 1996). Analysis by size-exclusion chromatography using a Waters Delta Prep 3000 HPLC equipped with a 300 SW column showed that the truncated E2o containing an N-terminal His tag eluted slightly before thyroglobulin (M_r = 640,000), whereas the truncated E2o containing a C-terminal His tag eluted near bovine gamma globulin (M_r = 158,000) (data not shown). These observations indicate that the former truncated E2o is a large oligomer, consistent with a calculated molecular weight of 895,000 for the 24-mer, whereas the latter truncated E2o appears to be a trimer. When analyzed by SDS-PAGE (data not shown), the trimer showed a major band with an anticipated molecular weight of ~37,000.

Crystallization and data collection

Conditions for the crystallization of the truncated E2o with the C-terminal His tag were screened by the sparse matrix technique (Cudney et al., 1994) using the hanging drop method (McPherson, 1990). The trimeric tE2o was found to crystallize using a precipitant solution of 1 M sodium acetate and 50 mM cadmium sulfate. The protein concentration was 20 mg/mL in 100 mM HEPES, pH 7.5. Crystals grew as hexagonal rods of ~0.3 mm in diameter and between 0.2 and 0.5 mm in length. One of the smaller crystals was rinsed with the precipitant solution before being dissolved in distilled water and subjected to amino-terminal sequencing at the University of Texas at Austin Protein Microanalysis Facility. This analysis detected a major component with the sequence ^{166}AQPA LAARSEKRVPM and a minor component with the sequence ^{172}AR SEKRVPMTRLRKE. This result indicates that the protein from the dissolved crystal lacks both the E3-binding domain and most of the adjacent linker region. A similar result was obtained in the crystallization of the 24-mer cE2o CD (Knapp et al., 1998), i.e., release of the E3-binding domain apparently by an endogenous protease or proteases, preceded crystallization of cE2o CD.

X-ray data were collected on a RAXIS IV image plate system equipped with a Rigaku RU-200 rotating anode generator operated at 50 kV and 110 mA (λ = 1.54 Å). Each image was collected at room temperature, using a crystal to film distance of 250 mm, an oscillation angle of 1.5°, and an exposure time of 20 min. The

initial X-ray analysis indicated that the E2o trimer crystals belong to a trigonal ($P3_121$) space group with cell dimensions of $a = b =$ 112.2 Å, and $c = 134.4$ Å. Assuming the presence of a trimer in the asymmetric unit, the Matthew's parameter is calculated to be V_m of 2.89 Å^3/Da. The measured intensities were processed with DENZO and merged with SCALEPACK (Otwinowski & Minor, 1997). The resulting data set of 18,677 reflections is 95.8% complete to 3.0 Å resolution with an overall multiplicity of 2.9, an overall R_{sym} of 10.3%, and an average $I/\sigma(I)$ of 13.8. Following the translation function, the correct space group was determined to be $P3_121$. Analysis of the data with the self-rotation function of GLRF (Tong & Rossmann, 1990) indicated that the molecular threefold axis is not parallel to the crystallographic threefold axis. Therefore, an intact trimer was used as the search model.

Structure determination

The phase problem was solved by the Molecular Replacement method using the routines of X-PLOR version 3.1 (Brünger, 1992a) running on a DEC ALPHA server. The search model was generated from one corner of the cubic form of the catalytic domain of the *E. coli* E2o (cE2o CD) (Knapp et al., 1998). This model consisted of three subunits, each related to the other by a crystallographic threefold symmetry operation. Between the rotation and translation functions, the Molecular Replacement protocol included a Patterson Correlation (PC) refinement step (Brünger, 1990), which allowed each of the subunits of the search model to be optimized by rigid body refinement. The cross-rotation function followed by the PC refinement resulted in a rotation solution at $\theta_1 = 7.4°$, $\theta_2 = 19.8°$, $\theta_3 = 28.9°$ (zxz Eulerian angles). The translation function produced a clear peak (26σ above the mean) at $x = 0.160$, $y = 0.960$, and $z = 0.420$ (in fractional coordinates). The positioned model had an initial *R*-factor of 0.441 for reflections between 10.0 and 3.5 Å resolution and a signal to noise greater than 2σ.

Refinement

After the molecular replacement solution, a set of 1,832 reflections (10% of all the reflections) was set aside to be used in the calculation of R_{free} (Brünger, 1992b). The tE2oCD model was then subjected to six rounds of X-PLOR refinement. During the first three rounds, strict NCS was used to constrain each subunit to be identical. During the last three rounds of refinement, the N-terminal residues (up to Lys186), part of helix H2 (residues 214–220), and the last few residues (residues 397–401) were refined without NCS restraints. Excluding these regions, the rest of the model was refined with tight NCS restraints (a NCS weight, W_{NCS} of 1,000).

A typical round of X-PLOR refinement included positional refinement using the conjugate gradient energy minimization (Powell, 1976) followed by optimization of main- and side-chain temperature factors for each residue. The last round of refinement included a bulk solvent correction step (Jiang & Brünger, 1994). Between each round of X-PLOR refinement, the model was fitted to either σ_A weighted $2F_o - F_c\ \alpha_{calc}$ or $F_o - F_c\ \alpha_{calc}$ electron density maps (Read, 1986) using the program "O" (Jones et al., 1991) running on a Silicon Graphics Crimson workstation. After each round of X-PLOR refinement and manual intervention, the quality of the stereochemistry of the model was monitored using the program PROCHECK (Laskowski et al., 1993). Regions of the structure with either questionable density or poor geometry were rebuilt into simulated annealing $2F_o - F_c$ and $F_o - F_c$ omit maps (Hodel et al., 1992). Solvent molecules were added to the model following the third round of X-PLOR refinement. Before the addition of solvent molecules, the tE2oCD model had an *R*-factor of 0.284 ($R_{free} = 0.323$) for all measured reflections between 10.0 and 3.0 Å resolution. During the last two rounds of refinement, the *B*-factors in the restrained region were constrained to be identical. Therefore, the *B*-factors in the restrained region represent the mean values calculated from the main- and side-chain *B*-factors of the equivalent residues located on the three NCS related subunits. In this way, the number of parameters was reduced without increasing R_{free}.

Analysis of the model

Least-squares superposition calculations were performed using LSQMAN (Kleywegt, 1996), and the results were displayed in "O" (Jones et al., 1991). The solvent accessible surface area was calculated using a 1.4 Å probe according to the method of Lee and Richards (1971) as implemented in the program SURFACE (CCP4, 1994). Intersubunit contacts were listed using the program CONTACT (CCP4, 1994). Figures 1, 2, and 5 were prepared using MOLSCRIPT (Kraulis, 1991). Figure 3 was made using the program MOLVIEW (Smith, 1992). Parts A and B of Figure 4 were prepared using Grasp (Nicholls et al., 1991). E2 sequences alignments were made using Macaw version 2.0.5 (Schuler et al., 1991). Coordinates of the tE2oCD have been deposited in the Protein Data Bank under the accession number 1c4t.

Acknowledgments

We are grateful to Dr. Klause Linsey for performing the N-terminal sequence analysis, to the staff at SSRL for helpful assistance with the data collection, and to Dr. Diane McCarthy for helpful comments on the preparation of this manuscript. This work was supported by Texas Advanced Research Program grant 003658-189 (M.L.H. & L.J.R.), Robert A. Welch Foundation grants F-1219 (M.L.H.), and F-1376 (L.J.R.) and U.S. Public Health Service Grants GM30105 (M.L.H.) and GM06590 (L.J.R.).

References

Ala' Aldeen DAA, Westphal AH, de Kok A, Weston V, Atta MS, Baldwin TJ, Bartley J, Borriello SP. 1996. Cloning, sequencing, characterization, and implications for vaccine design of the novel dihydrolipoyl acetyltransferase of *Neisseria meningitidis*. *J Med Microbiol 45*:419–432.

Ali G, Wasco W, Cai X, Szabo P, Kwan-Fu, RS, Cooper AJL, Gaston SM, Gusella JF, Tanzi RE, Blass JP. 1994. Isolation, characterization, and mapping of gene encoding dihydrolipoyl succinyltransferase (E2k) of human α-ketoglutarate dehydrogenase complex. *Somatic Cell Mol Genet 20*:94–105.

Berg A, Vervoort J, de Kok A. 1996. Solution structure of the lipoyl domain from the dihydrolipoyl succinyltransferase component of the 2-oxoglutarate dehydrogenase complex from *Azotobacter vinelandii*. *J Mol Biol 261*: 432–442.

Borges A, Hawkins CF, Packman LC, Perham RN. 1990. Cloning and sequence analysis of the genes encoding the dihydrolipoamide acetyltransferase and dihydrolipoamide dehydrogenase components of the pyruvate dehydrogenase complex of *Bacillus stearothermophilus*. *Eur J Biochem 194*:95–102.

Brünger AT. 1990. Extension of molecular replacement: A new search strategy based on Patterson refinement. *Acta Crystallogr A 46*:46–57.

Brünger AT. 1992a. *X-PLOR manual*, version 3.1. New Haven, Connecticut: Yale University Press.

Brünger AT. 1992b. Free R value: A novel statistical quantity for assessing the accuracy of crystal structures. *Nature 355*:472–475.

Burns G, Brown T, Hatter K, Sokatch JR. 1988. Comparison of the amino acid sequences of the transacylase components of branched-chain oxoacid dehydrogenase of *Pseudomonas putida* and the pyruvate and 2-oxoglutarate dehydrogenases of *Escherichia coli*. *Eur J Biochem 176*:165–169.

Carlsson P, Hederstedt L. 1989. Genetic characterization of *Bacillus subtilis odhA* and *odhB*, encoding 2-oxoglutarate dehydrogenase and dihydrolipoamide transsuccinylase, respectively. *J Bacteriol 171*:3667–3672.

CCP4 (Collaborative Computational Project Number 4). 1994. The CCP4 suite: Programs for protein crystallography. *Acta Crystallogr D 50*:760–763.

Cudney R, Patel S, Weisgraber K, Newhouse Y, McPherson A. 1994. Screening and optimization strategies for macromolecular crystal growth. *Acta Crystallogr D50*:414–423.

Dardel F, Davis AL, Laue ED, Perham RN. 1993. Three-dimensional structure of the lipoyl domain from *Bacillus stearothermophilus* pyruvate dehydrogenase multienzyme complex. *J Mol Biol 229*:1037–1048.

Fleischmann RD, Adams MD, White O, Clayton RA, Kirkness EF, Kerlavage AR, Bult CJ, Tomb J-F, Dougherty BA, Merrick JM, et al. 1995. Whole-genome random sequencing and assembly of *Haemophilus influenzae* Rd. *Science 269*:496–512.

Gibbs MR, Moody PCE, Leslie AGW. 1990. Crystal structure of the aspartic acid-199 → asparagine mutant of chloramphenicol acetyltransferase to 2.35 Å resolution: Structural consequences of disruption of a buried salt bridge. *Biochemistry 29*:11261–11265.

Green JDF, Laue ED, Perham RN, Ali ST, Guest JR. 1995. Three-dimensional structure of a lipoyl domain from the dihydrolipoyl acetyltransferase component of the pyruvate dehydrogenase multienzyme complex of *Escherichia coli*. *J Mol Biol 248*:328–343.

Griffin TA, Lau KS, Chuang DT. 1988. Characterization and conservation of the inner E2 core domain structure of branched-chain α-keto acid dehydrogenase complex from bovine liver. *J Biol Chem 263*:14008–14014.

Guest JR. 1987. Functional implications of structural homologies between chloramphenicol acetyltransferase and dihydrolipoamide acetyltransferase. *FEMS Microbiol Lett 44*:417–422.

Hanemaaijer R, Janssen A, de Kok A, Veeger C. 1988. The dihydrolipoyltransacetylase component of the pyruvate dehydrogenase complex from *Azotobacter vinelandii*, molecular cloning and sequence analysis. *Eur J Biochem 174*:593–599.

Hein S, Steinbüchel A. 1994. Biochemical and molecular characterization of the *Alcaligenes eutrophus* pyruvate dehydrogenase complex and identification of a new type of dihydrolipoamide dehydrogenase. *J Bacteriol 176*:4394–4408.

Hein S, Steinbüchel A. 1996. Cloning and characterization of the *Alcaligenes eutrophus* 2-oxoglutarate dehydrogenase complex. *FEMS Microbiol Lett 136*:231–238.

Hendle J, Mattevi A, Westphal AH, Spee J, de Kok A, Teplyakov A, Hol WGJ. 1995. Crystallographic and enzymatic investigations on the role of Ser558, His610, and Asn614 in the catalytic mechanism of *Azotobacter vinelandii* dihydrolipoamide acetyltransferase (E2p). *Biochemistry 34*:4267–4298.

Hodel A, Kim S-H, Brünger AT. 1992. Model bias in macromolecular crystal structures. *Acta Crystallogr A 48*:851–858.

Izard T, Aevarsson A, Allen MD, Westphal AH, Perham RN, de Kok A, Hol WG. 1999. Principles of quasi-equivalence and Euclidean geometry govern the assembly of cubic and dodecahedral cores of pyruvate dehydrogenase complexes. *Proc Natl Acad Sci USA 96*:1240–1245.

Jiang J-H, Brünger AT. 1994. Protein hydration observed by X-ray diffraction: Solvation properties of penicillopepsin and neuraminidase crystal structure. *J Mol Biol 243*:100–115.

Jones TA, Zou J-Y, Cowan SW, Kjeldgaard M. 1991. Improved methods for building protein models in electron density maps and the location of errors in these models. *Acta Crystallogr A 47*:110–119.

Kalia YN, Brocklehurst, SM, Hipps DS, Appella E, Sakaguchi K, Perham RN. 1993. The high-resolution structure of the peripheral subunit binding domain of dihydrolipoamide acetyltransferase from the pyruvate dehydrogenase multienzyme complex of *Bacillus stearothermophilus*. *J Mol Biol 230*:323–341.

Kleywegt GJ. 1996. Use of non-crystallographic symmetry in protein structure refinement. *Acta Crystallogr D 52*:842–857.

Knapp JE, Mitchell DT, Yazdi MA, Ernst SR, Reed LJ, Hackert ML. 1998. Crystal structure of the truncated cubic core component of the *Escherichia coli* 2-oxo-glutarate dehydrogenase multienzyme complex. *J Mol Biol 280*:655–668.

Knight R Jr, Gunsalus IC. 1962. Formation and breakdown of acyl lipoic acid. *Methods Enzymol 5*:651–656.

Kraulis PJ. 1991. MOLSCRIPT: A program to produce both detailed and schematic plots of protein structures. *J Appl Crystallogr 24*:946–950.

Laskowski RA, MacArthur MW, Moss DS, Thornton JM. 1993. PROCHECK: A program to check the stereochemical quality of protein structures. *J Appl Crystallogr 26*:283–291.

Lau KS, Chuang JL, Herring WJ, Danner DJ, Cox RP, Chuang DT. 1992. The complete cDNA sequence for dihydrolipoyl transacylase (E2) of human branched-chain α-keto acid dehydrogenase complex. *Biochim Biophys Acta 1132*:319–321.

Lee B, Richards FM. 1971. The interpretation of protein structures: Estimation of static accessibility. *J Mol Biol 55*:379–400.

Leslie AGW, Moody PCE, Shaw WV. 1988. Structure of chloramphenicol acetyltransferase at 1.75 Å resolution. *Proc Natl Acad Sci USA 85:*4133–4137.

Lewendon A, Murray IA, Kleanthous C, Cullis PM, Shaw WV. 1988. Substitution in the active site of chloramphenicol acetyltransferase: Role of a conserved aspartate. *Biochemistry 27*:7385–7390.

Maeng C-Y, Yazdi MA, Reed LJ. 1996. Stoichiometry of binding of mature and truncated forms of the dihydrolipoamide dehydrogenase-binding protein to the dihydrolipoamide acetyltransferase core of the pyruvate dehydrogenase complex from *Saccharomyces cerevisiae*. *Biochemistry 35*:5879–5882.

Mattevi A, Obmolova G, Kalk KH, Teplyakov A, Hol WGJ. 1993a. Crystallographic analysis of substrate binding and catalysis in dihydrolipoyl transacetylase (E2p). *Biochemistry 32*:3887–3901.

Mattevi A, Obmolova G, Kalk KH, Westphal AH, de Kok A, Hol WGJ. 1993b. Refined crystal structure of the catalytic domain of dihydrolipoyl transacetylase (E2p) from *Azotobacter vinelandii* at 2.6 Å resolution. *J Mol Biol 230*:1183–1199.

Mattevi A, Obmolova G, Schulze E, Kalk KH, Westphal AH, de Kok A, Hol WGJ. 1992. Atomic structure of the cubic core of the pyruvate dehydrogenase multienzyme complex. *Science 255*:1544–1550.

McPherson A. 1990. Current approaches to macromolecular crystallization. *Eur J Biochem 189*:1–23.

Nakano K, Matuda S, Sakamoto T, Takase C, Nakagawa S, Ohta S, Ariyama T, Inazawa J, Abe T, Miyata T. 1993. Human dihydrolipoamide succinyltransferase: cDNA cloning and localization on chromosome 14q24.2-q24.3. *Biochim Biophys Acta 1216*:360–368.

Nicholls A, Sharp KA, Honig B. 1991. Protein folding and association: Insights from the interfacial and thermodynamic properties of hydrocarbons. *Proteins Struct Funct Genet 11*:281–296.

Niu X-D, Browning KS, Behal RH, Reed LJ. 1988. Cloning and nucleotide sequence of the gene for dihydrolipoamide acetyltransferase from *Saccharomyces cerevisiae*. *Proc Natl Acad Sci USA 85*:7546–7550.

Otwinowski Z, Minor W. 1997. Processing of X-ray diffraction data collected in oscillation mode. *Methods Enzymol 276*:307–326.

Patel MS, Roche TE. 1990. Molecular biology and biochemistry of pyruvate dehydrogenase complexes. *FASEB J 4*:3224–3233.

Perham RN. 1991. Domains, motifs, and linkers in 2-oxo acid dehydrogenase multienzyme complexes: A paradigm in the design of a multifunctional protein. *Biochemistry 30*:8501–8512.

Philipp WJ, Poulet S, Eigleier K, Pascopella L, Balasubramanian V, Heym B, Bergh S, Bloom BR, Jacobs WR Jr, Cole ST. 1996. An integrated map of the genome of tubercle bacillus *Mycobacterium tuberculosis* H37Rv, and comparison with *Mycobacterium leprae*. *Proc Natl Acad Sci USA 93*:3132–3137.

Powell MJD. 1976. Some convergence properties of the conjugate gradient method. *Mathemat Program 11*:42–49.

Rae JL, Cutfield JF, Lamont IL. 1997. Sequences and expression of pyruvate dehydrogenase genes from *Pseudomonas aeruginosa*. *J Bacteriol 179*:3561–3571.

Read RJ. 1986. Improved Fourier coefficients for maps using phases from partial structures with errors. *Acta Crystallogr A 42*:140–149.

Reed LJ, Hackert ML. 1990. Structure–function relationships in dihydrolipoamide acyltransferases. *J Biol Chem 265*:8971–8984.

Repetto B, Tzagoloff A. 1990. Structure and regulation of KGD2, the structural gene for yeast dihydrolipoyl transsuccinylase. *Mol Cell Biol 10*:4221–4232.

Ricaud PM, Howard MJ, Roberts EL, Broadhurst RW, Perham RN. 1996. Three-dimensional structure of the lipoyl domain from the dihydrolipoyl succinyltransferase component of the 2-oxoglutarate dehydrogenase multienzyme complex of *Escherichia coli*. *J Mol Biol 264*:179–190.

Richardson JS. 1981. The anatomy and taxonomy of protein structure. *Adv Protein Chem 34*:167–339.

Robien MA, Clore GM, Omichinski JG, Perham RN, Appella E, Sakaguchi K, Gronenborn AM. 1992. Three-dimensional solution structure of the E3-binding domain of the dihydrolipoamide succinyltransferase core from the 2-oxoglutarate dehydrogenase multienzyme complex of *Escherichia coli*. *Biochemistry 31*:3463–3471.

Schuler GD, Altschul SF, Lipman DJ. 1991. A workbench for multiple alignment construction and analysis. *Proteins Struct Funct Genet 9*:180–190.

Shaw WV, Leslie AGJ. 1991. Chloramphenicol acetyltransferase. *Annu Rev Biophys Biophys Chem 20*:363–386.

Smith T. 1992. MacInPlot II—An updated program to display electron density and atomic models on the Macintosh personal computer. *J Appl Crystallogr 26*:496–498.

Spencer ME, Darlison MG, Stephens PE, Duckenfield IK, Guest JR. 1984. Nucleotide sequence of the sucB gene encoding the dihydrolipoamide succinyltransferase of *Escherichia coli* K12 and homology with the corresponding acetyltransferase. *Eur J Biochem 141*:361–374.

Stephens PE, Darlison MG, Lewis HM, Guest JR. 1983. The pyruvate dehydrog-

enase complex of *Escherichia coli* K12, nucleotide sequence encoding the dihydrolipoamide acetyltransferase component. *Eur J Biochem 133*:481–489.

Thekkumkara TJ, Ho L, Wexler, ID, Pons G, Liu T-C, Patel MS. 1988. Nucleotide sequence of a cDNA for the dihydrolipoamide acetyltransferase component of human pyruvate dehydrogenase complex. *FEBS Lett 240*:45–48.

Tong L, Rossmann MG. 1990. The locked rotation function. *Acta Crystallogr A46*:783–792.

Usuda Y, Tujimoto N, Abe C, Asakura Y, Kimura E, Kawahara Y, Kurahashi O, Matsui H. 1996. Molecular cloning of the *Corynebacterium glutamicum* ("Brevibacterium lactofermentum" AJ12036) *odhA* gene encoding a novel type of 2-oxoglutarate dehydrogenase. *Microbiology 142*:3347–3354.

Wang G-F, Kuriki T, Roy KL, Kaneda T. 1993. The primary structure of branched-chain α-oxo acid dehydrogenase from *Bacillus subtilis* and its similarity to other α-oxo acid dehydrogenases. *Eur J Biochem 213*:1091–1099.

Westphal AH, de Kok A. 1990. The 2-oxoglutarate dehydrogenase complex from *Azotobacter vinelandii* 2. Molecular cloning and sequence analysis of the gene encoding the succinyltransferase component. *Eur J Biochem 187*:235–239.